



PAPER

Quantum theory of continuum optomechanics

OPEN ACCESS

RECEIVED
25 June 2017REVISED
30 October 2017ACCEPTED FOR PUBLICATION
1 February 2018PUBLISHED
13 April 2018

Original content from this work may be used under the terms of the [Creative Commons Attribution 3.0 licence](#).

Any further distribution of this work must maintain attribution to the author(s) and the title of the work, journal citation and DOI.

Peter Rakich¹ and Florian Marquardt^{2,3,4} ¹ Department of Applied Physics, Yale University, New Haven, CT 06520, United States of America² Max Planck Institute for the Science of Light, Staudtstr. 2, D-91058, Erlangen, Germany³ Department of Physics, University of Erlangen-Nuremberg, Staudtstr. 7, D-91058, Erlangen, Germany⁴ Author to whom any correspondence should be addressed.E-mail: Florian.Marquardt@mpl.mpg.de

Keywords: optomechanics, waveguides, quantum optics

Abstract

We present the basic ingredients of continuum optomechanics, i.e. the suitable extension of cavity-optomechanical concepts to the interaction of photons and phonons in an extended waveguide. We introduce a real-space picture and argue which coupling terms may arise in leading order in the spatial derivatives. This picture allows us to discuss quantum noise, dissipation, and the correct boundary conditions at the waveguide entrance. The connections both to optomechanical arrays as well as to the theory of Brillouin scattering in waveguides are highlighted. Among other examples, we analyze the ‘strong coupling regime’ of continuum optomechanics that may be accessible in future experiments.

1. Introduction

Cavity optomechanics [1] is a very active research area at the interface of nanophysics and quantum optics. Its aim is to exploit radiation forces to couple optical and vibrational modes in a confined geometry, with applications ranging from sensitive measurements, wavelength conversion, and squeezing all the way to fundamental quantum physics. The paradigmatic cavity-optomechanical system is effectively zero-dimensional, i.e. there is no essential notion of spatial distance or dimensionality.

However, even though the vast majority of optomechanical systems rely on a cavity, there are a number of implementations that evade this paradigm. In particular, optomechanical effects are observed in waveguide-type structures, where both the optical field and the vibrations propagate in 1D, with the potential to uncover new classical and quantum phenomena. Examples include waveguides fabricated on a chip [2, 3] and thin membranes suspended in hollow-core fibres [4]. There have also been hybrid approaches, e.g., where the light propagates along the waveguide but couples to a localized mechanical mode [5], or with acoustic waves in whispering-gallery microresonators [6–8].

Coupling light and sound inside a waveguide has long been the subject of studies on Brillouin and Raman scattering in fibres [9–12]. This connection, between Brillouin physics and optomechanics, has recently been recognized as potentially fertile, and during the past year, first theoretical studies emphasizing this connection have emerged. The cavity-optomechanical coupling in a torus has been derived by starting from the known description of Brillouin interactions in an infinitely extended waveguide [13]. Conversely, the Hamiltonian coupling light and sound in such waveguides has been derived starting from the microscopic optomechanical interaction [14–17], including both boundary and photoelastic terms and fully incorporate geometric and material properties of the system. These works represent important bridges between the rapidly developing field of optomechanics and the significantly more advanced field of Brillouin scattering.

Independently, the role of dimensionality has also been emphasized for several years now in another area of optomechanics: discrete optomechanical arrays, i.e. periodic lattices of coupled optical and vibrational modes. These could be implemented in various settings, including photonic crystals [18], coupled optical disk resonators [19], or stacks of membranes. Recent theoretical studies have predicted interesting features, like photon–phonon polariton bandstructures [20–22], synchronization and nonlinear dynamics [23], long-range coupling [24–26], quantum many-body physics [27], artificial gauge fields, and topological transport [28–30].

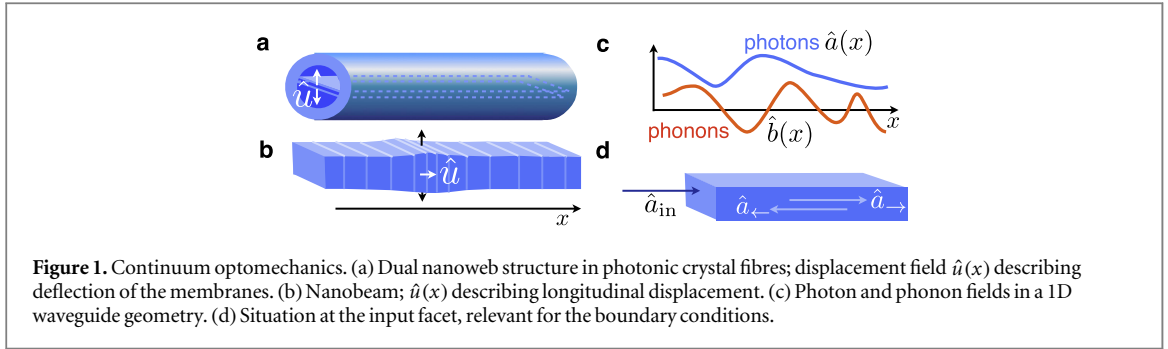


Figure 1. Continuum optomechanics. (a) Dual nanoweb structure in photonic crystal fibres; displacement field $\hat{u}(x)$ describing deflection of the membranes. (b) Nanobeam; $\hat{u}(x)$ describing longitudinal displacement. (c) Photon and phonon fields in a 1D waveguide geometry. (d) Situation at the input facet, relevant for the boundary conditions.

In the present manuscript, our aim is to establish a simple framework for ‘continuum optomechanics’, i.e., optomechanics in 1D waveguides without cavity modes, and to phrase it in a language that is as close as possible to the well-known cavity optomechanics case [1]. (i) We introduce a real-space picture and discuss how one can enumerate the possible coupling terms to leading order in spatial derivatives. (ii) We show how the continuum limit arises starting from discrete optomechanical arrays, thereby connecting Brillouin physics and these lattice structures. (iii) We include dissipation and quantum noise, deriving the quantum Langevin equations and the boundary conditions at the input of the waveguide. (iv) We discuss the ‘strong coupling regime’ that may be accessible in the future. (v) We provide an overview of experimentally achieved coupling parameters.

2. Continuum optomechanics in a real-space formulation

The usual cavity-optomechanical interaction Hamiltonian connects the photon field \hat{a} of a localized optical mode and the phonon field \hat{b} of a localized vibrational mode. It is of the parametric form [1]

$$-\hbar g_0 \hat{a}^\dagger \hat{a} (\hat{b} + \hat{b}^\dagger). \quad (1)$$

Our goal is to generalize this in the most straightforward way to the case of 1D continuum fields. We will do so in real-space, using phenomenological considerations.

To avoid confusion, we point out that our goal is specifically *not* to provide a microscopic derivation of coupling constants. Rather, we stay close to the spirit of cavity optomechanics, where the microscopic calculation of g_0 is left as a separate task, while the general form of the equations is universal. For an evaluation of the coupling constants for particular geometries one would resort to microscopic approaches, such as those presented recently in [14–16, 31]. While these approaches are powerful, and necessary to design an experimental system, they are involved and rather complex as an entry point into continuum optomechanics. Therefore, a phenomenological analysis can be useful in its own right. For many purposes, the level of detail provided here will be sufficient and reveal the essential features more easily. Moreover, a real-space picture is particularly useful in spatially inhomogeneous situations, such as those brought about by disorder, design, or nonlinear structure formation.

We introduce photon and phonon fields $\hat{a}(x)$ and $\hat{b}(x)$, respectively, for the waveguide geometry that we have in mind (figure 1). In contrast to prior treatments, we do not assume the fields to be sharply peaked around a particular wavevector [14–17]. This keeps our approach general and simplifies the representation of the interacting fields, especially for situations with strongly nonlinear dynamics. For example, this approach avoids the need to treat cascaded forward-scattering with an infinite number of photon fields, similar to the approach taken in [32]. The fields are normalized such that the total photon number in the entire system would be $\int dx \hat{a}^\dagger(x) \hat{a}(x)$, and likewise for the phonons. In addition, the fields obey the usual bosonic commutation relations for a 1D field, e.g. $[\hat{a}(x), \hat{a}^\dagger(x')] = \delta(x - x')$. For a nearly monochromatic wave packet of frequency ω , the energy density at position x is $\hbar\omega \langle \hat{a}^\dagger(x) \hat{a}(x) \rangle$, and the power can be obtained by multiplying this by the group velocity. The plane-wave normal modes would be $\hat{a}(k) = \int (dx/\sqrt{2\pi}) e^{-ikx} \hat{a}(x)$, with $[\hat{a}(k), \hat{a}^\dagger(k')] = \delta(k - k')$.

In the usual cavity-optomechanical situation, the displacement of the mechanical resonator would be $\hat{u} = \hat{b} + \hat{b}^\dagger$, if we normalize it via dividing by the zero-point fluctuation amplitude. Likewise, in the present situation, using our definition of the continuous phonon field $\hat{b}(x)$ introduced above, the normalized mechanical displacement field can be written as $\hat{u}(x) = \hat{b}(x) + \hat{b}^\dagger(x)$. In the most straightforward case, the physical displacement at any given point will then be obtained by multiplying with a suitable (three-dimensional, vectorial) mode function. In some of the simplest cases, discussed further below, $\hat{u}(x)$ is directly equal to the physical displacement, up to a constant prefactor (this prefactor has the dimensions of $\text{length}^{3/2}$, since \hat{b} has the dimension $\text{length}^{-1/2}$).

As is well-known from standard cavity optomechanics, any arbitrariness (e.g. in terms of the coupling) arising from the mode function normalization is avoided by formulating everything in terms of $\hat{a}(x)$ and $\hat{b}(x)$

(or equivalently $\hat{u}(x)$), since their normalization is directly tied to the overall energy in the system. Therefore, this is what we will do in the following.

The most obvious continuum optomechanical interaction can be written down as a direct generalization of the cavity case:

$$\hat{H}_{\text{int}} = -\hbar\tilde{g}_0 \int dx \hat{a}^\dagger(x) \hat{a}(x) \hat{u}(x). \quad (2)$$

Here \tilde{g}_0 defines the *continuum* optomechanical coupling constant, which replaces the usual single-photon cavity-optomechanical coupling g_0 . We note that \tilde{g}_0 has dimensions of frequency times the square root of length. Its meaning can be understood best in the following way: If there is a mechanical deflection $\langle \hat{b} \rangle = 1/\sqrt{l}$, corresponding to 1 phonon per length l , then the energy of any photon is shifted by $-\hbar\tilde{g}_0 2/\sqrt{l}$. We will comment more on the \sqrt{l} dependence when we make the connection to discrete optomechanical arrays.

While equation (2) is a plausible ansatz, it turns out to be only a part of the full interaction. Specifically, in a real-space formulation of the continuum case, derivative terms may appear, which we will now discuss.

Both boundary and bulk terms contribute to the optical frequency shift when a dielectric is deformed, as is well-known for optomechanics and has also been discussed recently in the present context [15, 16]. The boundary terms are proportional to the displacement \hat{u} , and their most natural representation is in the form of equation (2), if \hat{u} represents the deflection of the boundary (but see below). The bulk terms (photoelastic response), however, depend only on the spatial derivatives of the displacement field. In particular, this also involves derivatives along the longitudinal (waveguide) direction, leading to an expression

$$\hat{H}_{\text{int}}^{++-} = -\hbar\tilde{g}_0^{++-} \int dx \hat{a}^\dagger(x) \hat{a}(x) \partial_x \hat{u}(x). \quad (3)$$

We have introduced a superscript $++-$ for the coupling constant, with $-$ referring to the derivative, since $\partial_x \hat{u}$ changes sign if we set $\hat{u}(x) \mapsto \hat{u}(-x)$.

It is important to note that the shape of the Hamiltonian depends on the physical meaning of the displacement \hat{u} , which is to some degree a matter of definition. We have to distinguish the full vector field $\hat{\vec{u}}(\vec{r})$, which is defined unambiguously, from the reduced one-dimensional field $\hat{u}(x)$ that forms the object of our analysis. As a concrete example, consider longitudinal waves on a nanobeam. The 1D field $\hat{u}(x)$ could then be defined as the longitudinal displacement, evaluated at the beam center (see figure 1(b), white arrow). In that case the density change (crucial for photoelastic coupling) is proportional to $\partial_x \hat{u}(x)$. At the same time, a finite Poisson ratio will lead to a lateral expansion of the beam (relevant for the moving-boundary type optomechanical coupling). The surface deflection will be proportional to the density change, and thus also be set by $\partial_x \hat{u}(x)$. However, we could have defined $\hat{u}(x)$ differently, namely to represent directly the surface deflection (figure 1(b), black arrows). In that case, the density change would be given by $\hat{u}(x)$. Two different, equally valid definitions of $\hat{u}(x)$ would thus lead to different expressions in the Hamiltonian.

Another typically encountered physical example would be transverse waves propagating along such a nanobeam waveguide. In that case, it is most natural to choose $\hat{u}(x)$ as the transverse displacement, and this would directly couple to the light field (as it defines the local distortion of the structure from its equilibrium position). Similarly, the ‘dual-web’ fibre structure of [33] (figure 1(a)) shows the same kind of coupling, since $\hat{u}(x)$ controls the separation between the two parallel membranes, which affects the local effective refractive index. In general, the microscopic three-dimensional displacement field may depend on both $\hat{u}(x)$ and $\partial_x \hat{u}(x)$, as can be seen for example in the textbook case of a surface-acoustic wave, whose longitudinal component can be written as a derivative of a 1D wave field, whereas its transverse component is directly proportional to the 1D wave field.

Besides derivatives $\partial_x \hat{u}$, we may also encounter derivatives of the electric field. It is well-known that electromagnetic waves inside matter can also have longitudinal components, which change sign upon inversion of the propagation direction (in contrast to the transverse fields). Consequently, the electromagnetic mode functions depend on the direction of the wavevector, i.e. $\vec{E}(\vec{r}) = \vec{E}_k(\vec{r}_\perp) \exp(ikx)$. Upon going to our reduced 1D real-space description, this dependence on the sign of k leads to terms that are the derivatives of the 1D field (since for $\hat{a}(x) = \hat{a} e^{ikx}$ we have $\partial_x \hat{a}(x) = ik\hat{a}(x)$).

Table 1 shows all the coupling terms that arise in a real-space model of continuum optomechanics, to leading order in the derivatives. The simplest choice, of equation (2), would be identified as $\tilde{g}_0 = g_0^{+++}$.

Note that even and odd terms cannot be present simultaneously, unless inversion symmetry is broken. As long as inversion symmetry is intact, we must be able to turn a solution $u(z, t)$ into an equally valid solution $u^{\text{new}}(z, t) = u(-z, t)$ obtained by spatial inversion (or, possibly, $u^{\text{new}}(z, t) = -u(-z, t)$, if u is odd under reflection, as is the case if u represents longitudinal displacement along the propagation direction). Mixing even and odd terms in the equations of motion would violate this condition.

As remarked above, one can choose the definition of the 1D field $\hat{u}(x)$ to select either the ‘even’ or the ‘odd’ representation. Note that the constants have different physical dimensions (e.g. g_0^{++-} is of dimensions $m^{3/2}$ Hz).

Table 1. Possible coupling terms (to leading order in the derivatives) for continuum optomechanics, formulated in real-space. The Hamiltonian is of the form $-\hbar \int dx (\dots)$, with the integrand (\dots) containing one or more terms displayed here.

Even coupling terms	Odd coupling terms
$g_0^{+++} \hat{a}^\dagger \hat{a} \hat{u}$	$g_0^{++-} \hat{a}^\dagger \hat{a} (\partial_x \hat{u})$
$g_0^{--++} (\partial_x \hat{a}^\dagger) (\partial_x \hat{a}) \hat{u}$	$g_0^{-++} (\partial_x \hat{a}^\dagger) \hat{a} \hat{u} + \text{h.c.}$
$g_0^{-+-} (\partial_x \hat{a}^\dagger) \hat{a} (\partial_x \hat{u}) + \text{h.c.}$	$g_0^{---} (\partial_x \hat{a}^\dagger) (\partial_x \hat{a}) (\partial_x \hat{u})$

Interaction terms with derivatives would also arise by starting from the microscopic theory, translating from k -space into real-space. In general, this could yield derivatives of any order. Here, our aim was to keep the leading terms, retaining qualitatively important features such as the difference between forward- and backward-scattering amplitudes (section 7).

Is our list complete? To answer this, let us discuss the ‘even’ sector only, without loss of generality. In this sector, we went up to second order in the derivatives, keeping terms such as $(\partial_x \hat{a}^\dagger) \hat{a} (\partial_x \hat{u})$. Why did we not consider second derivatives of individual fields, like $\hat{a}^\dagger \hat{a} (\partial_x^2 \hat{u})$? The answer is that these can indeed be present. However, a simple integration by parts will transform those terms into a combination of the terms that we already listed.

Beyond the interaction, the Hamiltonian contains the unperturbed energy of the photons, $\hat{H}_a = \int dk \hbar \omega(k) \hat{a}^\dagger(k) \hat{a}(k)$, and likewise \hat{H}_b for the phonons with their dispersion $\Omega(k)$. In real-space, the same term could be written as $\hat{H}_a = \hbar \int dx \hat{a}^\dagger(x) \omega(-i\partial_x) \hat{a}(x)$, where $\omega(-i\partial_x)$ applied to e^{ikx} will reproduce $\omega(k)$.

The resulting coupled continuum optomechanical Heisenberg equations of motion take the form:

$$\partial_t \hat{a} = -i\omega(-i\partial_x) \hat{a} + i\tilde{g}_0 \hat{a} (\hat{b} + \hat{b}^\dagger) \quad (4)$$

$$\partial_t \hat{b} = -i\Omega(-i\partial_x) \hat{b} + i\tilde{g}_0 \hat{a}^\dagger \hat{a}. \quad (5)$$

Here, equations (4) and (5) are expressed with the simple interaction. More generally, the interaction may be comprised of a linear combination of terms in table 1. For example, the term $i\tilde{g}_0 \hat{a} (\hat{b} + \hat{b}^\dagger)$ in equation (4) becomes

$$\begin{aligned} & i\tilde{g}_0^{+++} \hat{a} \hat{u} - i\tilde{g}_0^{--++} \partial_x (\hat{u} \partial_x \hat{a}) \\ & - i\tilde{g}_0^{-+-} \partial_x (\hat{a} \partial_x \hat{u}) + i\tilde{g}_0^{-+-*} (\partial_x \hat{a}) (\partial_x \hat{u}) \end{aligned} \quad (6)$$

when even couplings are considered. Likewise, term $i\tilde{g}_0 \hat{a}^\dagger \hat{a}$ of equation (5) becomes

$$\begin{aligned} & i\tilde{g}_0^{+++} \hat{a}^\dagger \hat{a} + i\tilde{g}_0^{--++} (\partial_x \hat{a}^\dagger) (\partial_x \hat{a}) \\ & - i\tilde{g}_0^{-+-} \partial_x ((\partial_x \hat{a}^\dagger) \hat{a}) - i\tilde{g}_0^{-+-*} \partial_x (\hat{a}^\dagger (\partial_x \hat{a})). \end{aligned} \quad (7)$$

The real-space formulation developed here, with the complete list of interactions derived above, will be especially powerful for considering the effects of nonlinearities and of spatial inhomogeneities (due to disorder or structure formation). No assumptions about the fields peaking around a certain wavevector have been employed, nor are we required to introduce a multitude of photon fields for cases like forward scattering. The classical version of these nonlinear equations can readily be solved by using split-step Fourier techniques.

3. Dissipation and quantum noise

So far, we have only discussed the terms that give rise to completely coherent dynamics. However, in a real system, dissipation of both photons and phonons is present. In addition, there is necessarily vacuum noise (and possibly thermal noise) entering the system via these dissipation channels. Therefore, we are dealing with an (extended) open quantum system.

To discuss the dissipation and the associated quantum and thermal noise, we employ the well-known input-output formalism and adapt it suitably to the continuum case. If we assume the photon loss rate to be κ , then the equation of motion contains additional terms

$$\partial_t \hat{a}(x, t) = \dots - \frac{\kappa}{2} \hat{a}(x, t) + \sqrt{\kappa} \hat{a}_{\text{in}}(x, t), \quad (8)$$

where the vacuum noise field \hat{a}_{in} obeys the commutation relation $[\hat{a}_{\text{in}}(x, t), \hat{a}_{\text{in}}^\dagger(x', t')] = \delta(x - x') \delta(t - t')$ and has the correlators $\langle \hat{a}_{\text{in}}(x, t) \hat{a}_{\text{in}}^\dagger(x', t') \rangle = \delta(x - x') \delta(t - t')$ and $\langle \hat{a}_{\text{in}}^\dagger(x', t') \hat{a}_{\text{in}}(x, t) \rangle = 0$. These ensure that the commutator of \hat{a} is preserved, i.e. the vacuum noise is constantly being replenished to offset the losses.

The mechanical field can be treated likewise, with a damping rate Γ in place of κ , and with the additional contribution of thermal noise: $\langle \hat{b}_{\text{in}}(x, t) \hat{b}_{\text{in}}^\dagger(x', t') \rangle = (\bar{n}_{\text{th}} + 1) \delta(x - x') \delta(t - t')$ and

$\langle \hat{b}_{\text{in}}^\dagger(x', t') \hat{b}_{\text{in}}(x, t) \rangle = \bar{n}_{\text{th}} \delta(x - x') \delta(t - t')$. Here $\bar{n}_{\text{th}} = (\exp(\hbar \Omega / k_B T) - 1)^{-1}$ is the occupation at temperature T . For simplicity, we assumed a fixed frequency Ω , since the phonon dispersion $\Omega(k)$ is usually nearly flat.

4. Boundary conditions

Besides the dissipation distributed along the extended 1D continuum optomechanical system (analyzed in the previous section), there are also the input and output ports at the ends of the waveguide. These require a separate treatment, which can be modeled after input–output theory as it is known for cavity systems.

We now turn to the driving and boundary terms. A laser injecting light of amplitude α_{in} at point x yields an additional term $\sqrt{\kappa_{\text{ex}}} \alpha_{\text{in}}(x, t)$ in equation (8), with $\alpha_{\text{in}}(x, t) = \alpha_{\text{in}}(x) e^{-i\omega_L t}$. Here κ_{ex} is the coupling to the field mode populated by the laser, and $\hbar\omega_L |\alpha_{\text{in}}(x, t)|^2$ is the power per unit length impinging on the waveguide at position x . This description is appropriate for illumination from the side, which is feasible but atypical in waveguide experiments.

More commonly, light is injected at the waveguide entrance. In that case, we consider a half-infinite system, starting at $x = 0$ and extending to the right (figure 1(d)). The boundary at $x = 0$ must be such that incoming waves (including the quantum vacuum noise) are perfectly launched into the waveguide as right-going waves, while left-moving waves exit without reflection. For the simplest case of a constant photon velocity c , we need to prescribe the right-going amplitude at $x = 0$,

$$\partial_t \hat{a}(0, t) - c \partial_x \hat{a}(0, t) = -\sqrt{\frac{2}{c}} \partial_t (\alpha_{\text{in}}(t) + \hat{a}_{\text{in}}(t)), \quad (9)$$

where the ingoing quantum noise has the correlator $\langle \hat{a}_{\text{in}}(t) \hat{a}_{\text{in}}^\dagger(0) \rangle = \delta(t)$, while $\langle \hat{a}_{\text{in}}^\dagger(t) \hat{a}_{\text{in}}(0) \rangle$ vanishes. Equation (9) is valid also in the presence of dissipation. The solution of the free wave equation $\partial_t^2 \hat{a} - c^2 \partial_x^2 \hat{a} = 0$ with the boundary condition (9) is

$$\hat{a}(x, t) = \hat{a}_{\rightarrow}(x - ct) + \hat{a}_{\leftarrow}(x + ct), \quad (10)$$

where the right-moving field is set by $\hat{a}_{\text{in}}(t)$:

$$\hat{a}_{\rightarrow}(x) = \hat{a}_{\text{in}}(x/c) / \sqrt{2c}. \quad (11)$$

The left-moving field is an independent fluctuating field. The correlator of the right-movers is

$$\begin{aligned} \langle \hat{a}_{\rightarrow}(x) \hat{a}_{\rightarrow}^\dagger(x') \rangle &= \frac{1}{2c} \langle \hat{a}_{\text{in}}(x/c) \hat{a}_{\text{in}}^\dagger(x'/c) \rangle \\ &= \frac{1}{2c} \delta\left(\frac{x - x'}{c}\right) = \frac{1}{2} \delta(x - x') \end{aligned}$$

and the same result holds for the left-movers, such that the full equal-time correlator of the $\hat{a}(x)$ field is set by $\delta(x - x')$.

5. Linearized description

So far, we have derived the full nonlinear quantum dissipative equations of motion for the coupled photon and phonon fields. However, in many situations we may simplify the analysis drastically by turning to a linearized description. As usual, this assumes that the field consists of a strong classical amplitude and some weak quantum fluctuations on top of it.

In a rotating frame, we have $\hat{a}^{\text{old}}(x, t) = \hat{a}^{\text{new}}(x, t) \cdot e^{i(k_L x - \omega_L t)}$, where $\omega_L = \omega(k_L)$ is the laser frequency. From now on, we drop the ‘new’; all \hat{a} are in the rotating frame. We get:

$$\partial_t \hat{a} = -i\tilde{\omega}(-i\partial_x) \hat{a} + \dots, \quad (12)$$

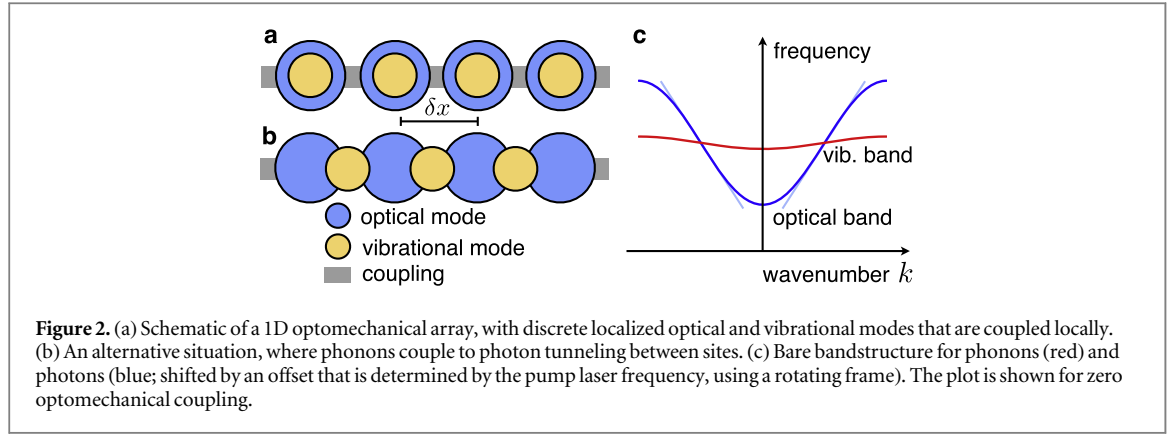
where we set $\tilde{\omega}(-i\partial_x) = \omega(k_L - i\partial_x) - \omega_L$. For fields with $k \approx k_L$, this may be expanded, using the group velocity $v = d\omega(k_L)/dk$:

$$\partial_t \hat{a} = -v \partial_x \hat{a} + \dots \quad (13)$$

The equation for the phonon field remains unaffected.

We linearize the equations (see appendix A) by setting $\beta(x) = \langle \hat{b}(x) \rangle$ and $\alpha(x) = \langle \hat{a}(x) \rangle$ for the steady-state solution, and $\delta \hat{b} = \hat{b} - \beta$ and $\delta \hat{a} = \hat{a} - \alpha$ for the fluctuations. Then we obtain (for the simplest interaction term):

$$\partial_t \delta \hat{a} = -i\tilde{\omega}(-i\partial_x) \delta \hat{a} + i\tilde{g}(\delta \hat{b} + \delta \hat{b}^\dagger) + i\tilde{g}_\beta \delta \hat{a} + \dots \quad (14)$$



$$\partial_t \delta \hat{b} = -i\Omega(-i\partial_x)\delta \hat{b} + i(\tilde{g}\delta \hat{a}^\dagger + \tilde{g}^*\delta \hat{a}) + \dots \quad (15)$$

Here we introduced the linearized coupling $\tilde{g}(x) \equiv \tilde{g}_0 \alpha(x)$, as well as the shift $\tilde{g}_j(x) \equiv \tilde{g}_0(\beta(x) + \beta^*(x))$. The omitted terms (...) in equations (14) and (15) contain the dissipation and fluctuations, in the same form as above (only with $\hat{a} \mapsto \delta \hat{a}$, and likewise for \hat{b}). The boundary conditions for the fluctuations $\delta \hat{a}$ do not contain any laser driving any more; i.e. we would have equation (9) for $\delta \hat{a}$, but without the laser amplitude α_{in} .

6. Continuum limit for optomechanical arrays

In this section, our aim is to relate the framework presented above to the well-developed theory of optomechanical arrays [23, 27–29]. We will show that the present system can be understood as the continuum limit of a discrete optomechanical array, where the lattice constant tends to zero. This should help to transfer insights between those two fields.

We consider an optomechanical array where discrete localized optical and vibrational modes are coupled to each other via the optomechanical interaction $-\hbar g_0 \hat{a}_j^\dagger \hat{a}_j (\hat{b}_j + \hat{b}_j^\dagger)$, see figure 2. In addition, the photon and phonon modes \hat{a}_j and \hat{b}_j are coupled by tunneling between neighboring sites. For the photons, in a 1D array, this is described by the tight-binding Hamiltonian $-\hbar \sum_{j,l} J_l \hat{a}_{j+l}^\dagger \hat{a}_j + \text{h.c.}$. Here J_l is the tunnel coupling connecting any two sites j and $j+l$. The resulting dispersion relation for the optical tight-binding band is $\omega(k) = -\sum_l e^{-ikl\delta x} J_l$, where we already introduced the lattice constant δx . For the phonons, an analogous Hamiltonian holds, with a coupling constant K_l and a resulting phononic band $\Omega(k)$.

The continuum approximation will be good if only long wavelengths (many lattice spacings) are excited. The properly normalized way to identify localized modes with the continuum fields is

$$\hat{a}_j = \hat{a}(j\delta x) \sqrt{\delta x}, \quad \hat{b}_j = \hat{b}(j\delta x) \sqrt{\delta x}. \quad (16)$$

This ensures the validity of the commutator relations such as $[\hat{a}(x), \hat{a}^\dagger(x')] = \delta(x - x')$. We then obtain

$$\hat{H}_{\text{int}}^{\text{array}} = -\hbar g_0 \sum_j \hat{a}_j^\dagger \hat{a}_j (\hat{b}_j + \hat{b}_j^\dagger) \approx \hat{H}_{\text{int}}^{\text{cont}}. \quad (17)$$

Here $\hat{H}_{\text{int}}^{\text{cont}}$ is the continuum version, see equation (2). For this simple local interaction, none of the ‘derivative-terms’ appears. We can now relate the coupling constants for the continuum and the discrete model:

$$\tilde{g}_0 = g_0 \sqrt{\delta x}. \quad (18)$$

In taking the proper continuum limit, \tilde{g}_0 has to be kept fixed, i.e. $g_0 \sim 1/\sqrt{\delta x}$ as $\delta x \rightarrow 0$. This is the expected physical behaviour, since $g_0 \sim x_{\text{ZPF}}$, where $x_{\text{ZPF}} = \sqrt{\hbar/(2m\Omega)}$ is the size of the mechanical zero-point fluctuations of a discrete mechanical mode. If this mode represents a piece of length δx in a continuous waveguide, its mass scales as $m = \delta x \cdot \rho$ (with ρ the mass density), such that g_0 grows in the manner discussed above when δx is sent to zero. Note that the continuum limit also means keeping $\omega(k)$ and $\Omega(k)$ fixed in the relevant wavelength range.

One can now also confirm that our treatment of quantum noise and dissipation corresponds to the input–output formalism applied to the discrete modes. For such modes, we would have $\dot{\hat{a}}_j = \dots - \frac{\kappa}{2} \hat{a}_j + \sqrt{\kappa} \hat{a}_{j,\text{in}}(t)$, with $\langle \hat{a}_{j,\text{in}}(t) \hat{a}_{j',\text{in}}^\dagger(0) \rangle = \delta_{j,j'} \delta(t)$ and $[\hat{a}_{j,\text{in}}, \hat{a}_{j',\text{in}}^\dagger] = \delta_{j,j'}$. Setting $\hat{a}_{j,\text{in}}(t) = \sqrt{\delta x} \hat{a}_{\text{in}}(j\delta x, t)$, this turns into the continuum expressions given above.

So far, we had assumed a local interaction of the type $-\hbar g_0 \hat{a}_j^\dagger \hat{a}_j (\hat{b}_j + \hat{b}_j^\dagger)$. However, it is equally possible to have an interaction that creates phononic excitations during the photon tunneling process:

$-\hbar g_0(\hat{a}_{j+1}^\dagger \hat{a}_j + \text{h.c.})\hat{u}_j$, where $\hat{u}_j \equiv \hat{b}_j + \hat{b}_j^\dagger$ describes the displacement of a mode attached to the link between the sites j and $j + 1$; see figure 2(b). It turns out that such a coupling gives rise to ‘derivative’ terms in the continuum model (see appendix B).

7. Elementary processes for a single optical branch

In this section, we now show how the various terms in the coupling Hamiltonian will appear in the simplest situation, where the scattering can be treated perturbatively and the system is translationally invariant (such that a k -space picture applies). This is useful to make the connection to standard perturbative treatments e.g. in nonlinear optics.

Translating the couplings in table 1 to k -space, we arrive at the substitutions $\hat{a}(x) \mapsto \hat{a}_k$, $\hat{a}^\dagger(x) \mapsto \hat{a}_{k+q}^\dagger$ and $\hat{u}(x) \mapsto \hat{u}_q$, with $\hat{u}_q = \hat{b}_q + \hat{b}_{-q}^\dagger$. In addition, $\partial_x \hat{a} \mapsto ik\hat{a}_k$, $\partial_x \hat{a}^\dagger \mapsto -i(k+q)\hat{a}_{k+q}^\dagger$, and $\partial_x \hat{u} \mapsto iq\hat{u}_q$. This yields the following amplitude (for the example of the ‘even’ sector) in front of the resulting term $\hat{a}_{k+q}^\dagger \hat{a}_k \hat{u}_q$ in the Hamiltonian:

$$-\hbar \{g_0^{+++} + g_0^{-++}(k+q)k + g_0^{-+-}(k+q)q - g_0^{-+-*}kq\}. \quad (19)$$

We can now specifically distinguish the amplitudes for forward-scattering ($q \approx 0$):

$$g_{0F} = g_0^{+++} + g_0^{-++}k^2 \quad (20)$$

and backward-scattering ($q \approx -2k$):

$$g_{0B} = g_0^{+++} - k^2 g_0^{-++} + 2k^2(g_0^{-+-} + g_0^{-+-*}). \quad (21)$$

Clearly it was important to keep more than the simplest interaction term g_0^{+++} in real-space to allow that these amplitudes are different.

The situation differs significantly from standard cavity optomechanics, if only forward-scattering is considered. The crucial asymmetry between Stokes and anti-Stokes processes is absent here in forward-scattering, where phonons of wavenumber q can be emitted and absorbed equally likely, scattering laser photons into a comb [4, 32, 34, 35] of sidebands $\omega_L \pm n\Omega$ with $\Omega = \Omega(q)$. As a consequence, basic phenomena in cavity optomechanics, like cooling or state transfer, do not translate to forward scattering with a single optical branch. The optical dispersion is rarely sufficient to introduce symmetry breaking, as typical propagation lengths are too small. More precisely, the slight remaining asymmetry due to the optical dispersion $d^2\omega/dk^2$ over the frequency range Ω is typically insufficient: the difference between Stokes and anti-Stokes wavenumbers, $\delta q = \Omega^2(d^2\omega/dk^2)/(d\omega/dk)^3$, is too small to be resolved in typical waveguide lengths (or decay/absorption lengths).

In backward scattering, the situation is entirely different, since either phonons of wavenumber $q \cong 2k_L$ are emitted (Stokes) or those of wavenumber $q \cong -2k_L$ are absorbed (anti-Stokes). This can result in cooling of $-2k_L$ phonons and amplification of $+2k_L$ phonons. The latter process amounts to stimulated backward Brillouin scattering, amplifying any counterpropagating beam.

8. Multiple optical branches

In a cavity-optomechanical system, interesting novel phenomena occur when one considers multiple optical modes. The same is true for continuum systems, where different transverse optical modes (possibly different polarization patterns) correspond to different optical branches of the dispersion relation. Analyzing them is particularly important in order to come closer to the physics known from cavities.

In particular, the useful Stokes/anti-Stokes asymmetry (useful for cooling, state transfer, and amplification) can be re-introduced into forward scattering by considering multiple optical branches. In that case, the (simplest) interaction is

$$-\hbar \sum_{j,l} \int dx \tilde{g}_0(j,l) \hat{a}_j^\dagger(x) \hat{a}_l(x) (\hat{b}(x) + \hat{b}^\dagger(x)). \quad (22)$$

Here $\tilde{g}_0(j,l)$ describes the bare coupling for scattering from branch l to j , with $\tilde{g}_0^*(l,j) = \tilde{g}_0(j,l)$, and $[\hat{a}_j(x), \hat{a}_l^\dagger(x')] = \delta_{jl} \delta(x-x')$. Analogous expressions can be written down for the other interactions of table 1.

For the case of two branches, there will be forward-scattering of photons $k_L \mapsto k_L + q$ between the branches, by either absorbing a phonon of wavenumber q or emitting one of wavenumber $-q$. In the linearized Hamiltonian, the inter-branch scattering process is described by

$$-\hbar \int dx (\tilde{g}_{21}(x) \delta \hat{a}_2^\dagger(x) + \text{h.c.}) (\delta \hat{b}(x) + \delta \hat{b}^\dagger(x)), \quad (23)$$

with $\tilde{g}_{21}(x) = \tilde{g}_{21} e^{ik_L x}$, where $\tilde{g}_{21} = \tilde{g}_0(2, 1)\alpha_1$. In momentum space, this turns into

$$-\hbar \int dq \tilde{g}_{21} \delta \hat{a}_2 [k_L + q]^\dagger (\delta \hat{b}[q] + \delta \hat{b}[-q]^\dagger) + \text{h.c.} \quad (24)$$

9. Interband scattering: weak coupling

In the present section, we review the weak coupling limit for interband scattering, to connect our formalism to the standard literature on this topic. In the case of forward scattering, this is known as stimulated intermodal Brillouin scattering (SIMS). In the case of backward scattering, one speaks of backward stimulated Brillouin scattering (see appendix C for naming conventions). This is a widely studied regime in the context of nonlinear optics [9, 11, 12, 36]. The phonon decay lengths are assumed to be far shorter than those for the photons, which is frequently satisfied experimentally. Then the effective nonlinear optical susceptibility is approximately local, greatly simplifying the spatio-temporal dynamics. For clarity, we term this regime the ‘Brillouin limit’.

To connect our framework with known results, we start from equation (23), for two optical branches. Just as in equations (12) and (13), we introduce rotating frames and linearize the dispersion. We now assume steady-state, i.e. the time-derivatives vanish. Then we obtain:

$$\partial_x \langle \delta \hat{a}_2 \rangle = i(\tilde{g}_{21}/\nu_2) \langle \delta \hat{b}^\dagger \rangle - (\gamma_2/2) \langle \delta \hat{a}_2 \rangle, \quad (25)$$

$$\partial_x \langle \delta \hat{b} \rangle = i(\tilde{g}_{21}/\nu_b) \langle \delta \hat{a}_2^\dagger \rangle - (\gamma_b/2) \langle \delta \hat{b} \rangle. \quad (26)$$

Note that we are dealing with the averages, since this is sufficient for the present analysis. Therefore the noise terms vanish. In addition, we introduced the notation $\gamma_2 \equiv \kappa_2/\nu_2$ and $\gamma_b \equiv \Gamma/\nu_b$, representing the spatial power decay rate of the photon (phonon) fields, i.e. the inverse decay length. Note that in treating \tilde{g}_{21} as a constant, we are neglecting pump depletion. This is valid as long as the power carried by the generated field $\delta \hat{a}_2$ remains much smaller than the incoming pump power.

Since we are assuming $\gamma_b \gg \gamma_2$, the phonon field is generated locally: $\partial_x \langle \delta \hat{b} \rangle \approx 0$. This allows to eliminate $\langle \delta \hat{b} \rangle$, which yields:

$$\partial_x \langle \delta \hat{a}_2 \rangle = \frac{|\tilde{g}_{21}|^2}{\nu_1 \Gamma} \langle \delta \hat{a}_2 \rangle - (\gamma_2/2) \langle \delta \hat{a}_2 \rangle. \quad (27)$$

We now cast this result in terms of traveling-wave optical powers P_1 and P_2 , with $P_1 = \hbar \omega_1 \nu_1 |\alpha_1|^2$, $P_2 \cong \hbar \omega_2 \nu_2 |\langle \delta \hat{a}_2 \rangle|^2$, and $P_b \cong \hbar \Omega \nu_b |\langle \delta \hat{b} \rangle|^2$. Here we assumed the small signal limit, i.e. $\alpha_2 = 0, \beta = 0$, and α_1 is large. We see that P_2 is exponentially amplified according to $\partial P_2 / \partial x = G_B P_1 P_2 - \gamma_2 P_2$, where

$$G_B \equiv 4|\tilde{g}_0(2, 1)|^2 / (\nu_1 \nu_2 \Gamma \hbar \omega_1) \quad (28)$$

is the Brillouin gain coefficient [2, 12]. For alternative derivations in the context of nonlinear optics and Brillouin photonics, see [11, 12] (for the induced nonlinear optical susceptibility, see appendix D). This relationship between G_B and $\tilde{g}_0(2, 1)$ permits us to leverage established methods for calculation of the optomechanical coupling in both translationally invariant [2, 15, 37, 38] and periodic [39] nano-optomechanical systems. In the Brillouin limit, a range of complex spatio-temporal phenomena have been studied [11, 12].

10. Strong coupling

The case opposite to the ‘Brillouin limit’, that we just discussed, is the situation of a large phonon coherence length, as can be achieved at low temperatures (e.g. see [40]). In this much less explored limit, a large variety of interesting classical and quantum phenomena can be expected to appear, as the system acquires a much higher degree of coherence and nonlocality. Quantum states can then be swapped between the light field and the phonon field, which can lead to applications like opto-acoustic data storage in a fibre [41].

We now consider the situation where creation of a photon in the second branch is accompanied by *absorption* of a phonon (now $\omega_2 > \omega_1$), instead of the emission that would lead to amplification. This leads to a modified version of equations (25) and (26). In contrast to (25), now the optical amplitude $\langle \delta \hat{a}_2 \rangle$ couples directly to the mechanical amplitude $\langle \delta \hat{b} \rangle$, instead of its Hermitian conjugate. We obtain:

$$\partial_x \langle \delta \hat{a}_2 \rangle = i(\tilde{g}_{21}/\nu_2) \langle \delta \hat{b} \rangle - (\gamma_2/2) \langle \delta \hat{a}_2 \rangle, \quad (29)$$

$$\partial_x \langle \delta \hat{b} \rangle = i(\tilde{g}_{21}^*/\nu_b) \langle \delta \hat{a}_2 \rangle - (\gamma_b/2) \langle \delta \hat{b} \rangle. \quad (30)$$

That can be recast as a matrix equation

$$\partial_x \phi = M \phi, \quad (31)$$

where the vector ϕ contains the fields, $\phi = (\langle \delta \hat{a}_2 \rangle, \langle \delta \hat{b} \rangle)^T$, and

$$M = \begin{pmatrix} -\gamma_2/2 & i\tilde{g}_{21}/v_2 \\ i\tilde{g}_{21}^*/v_b & -\gamma_b/2 \end{pmatrix}. \quad (32)$$

This is a non-Hermitian matrix that can be diagonalized to obtain the spatial evolution $\phi \sim e^{\lambda x}$. We find the eigenvalues

$$\lambda_{\pm} = \frac{1}{2}[-\bar{\gamma} \pm \sqrt{D}], \quad (33)$$

where $\bar{\gamma} = (\gamma_2 + \gamma_b)/2$ is the average spatial decay rate, and $D = [(\gamma_2 - \gamma_b)/2]^2 - 4|\tilde{g}_{21}|^2/v_2 v_b$. A distinct oscillatory regime is reached when $D < 0$, i.e.

$$|\tilde{g}_{21}| > \sqrt{v_2 v_b} \frac{|\gamma_2 - \gamma_b|}{4}. \quad (34)$$

In that case, the eigenvalues attain an imaginary part, and the spatial evolution becomes oscillatory. This oscillatory evolution has recently also been pointed out in the context of a detailed discussion of Brillouin cooling in a linear waveguide [42]. Interestingly, this sharp threshold only depends on the *difference* of spatial decay rates. In principle, therefore, in an unconventional system where γ_2 and γ_b are of the same order, this condition is much easier to fulfill than when having to compare $|\tilde{g}_{21}|$ against the total decay rate. Nevertheless, in order for the oscillations to be observed in practice, in addition the decay length should be larger than the period of oscillations. This will be true when $|\operatorname{Re} \lambda| \ll |\operatorname{Im} \lambda|$, which can be approximated as

$$|\tilde{g}_{21}| \gg \sqrt{v_2 v_b} \bar{\gamma}/2. \quad (35)$$

One may call this the ‘*strong coupling regime*’ for continuum optomechanics. This strong coupling regime of continuum optomechanics has also been discussed recently in [13], in terms of a mapping between a cavity-optomechanical system (a finite waveguide resonator forming a cavity) and the continuum situation. It is in spirit similar to the strong coupling regime of cavity optomechanics [1], although the dependence on the velocities introduces a new element. If this more demanding condition (35) is fulfilled, then the coupling is also automatically larger than the threshold (34) given above. To interpret this condition, note that usually $\bar{\gamma}$ is dominated by the phonon decay $\gamma_b = \Gamma/v_b$. In that case, we could also write $|\tilde{g}_{21}| \gg \sqrt{v_2/v_b} \Gamma/4$. This shows that, at a fixed phonon decay rate Γ , smaller phonon velocities make the strong coupling regime harder to reach.

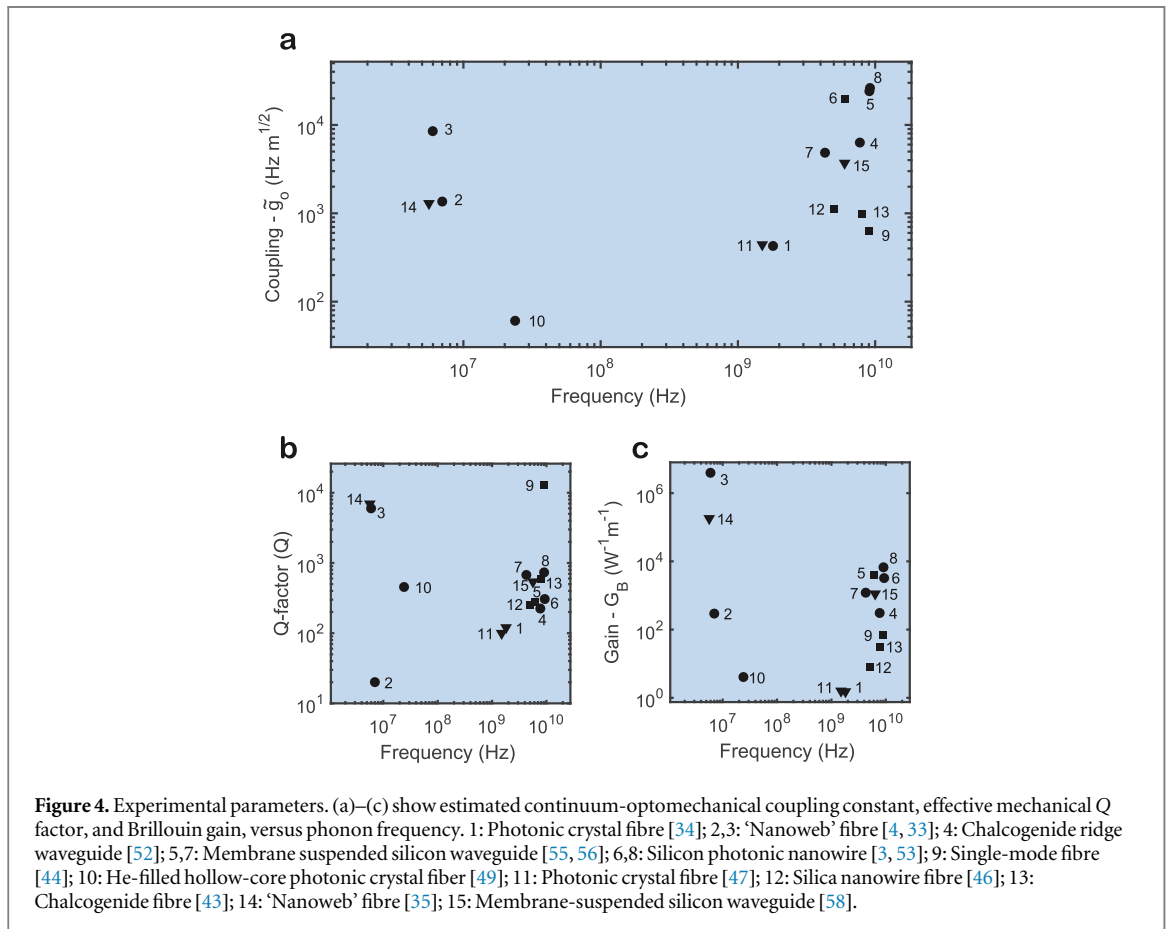
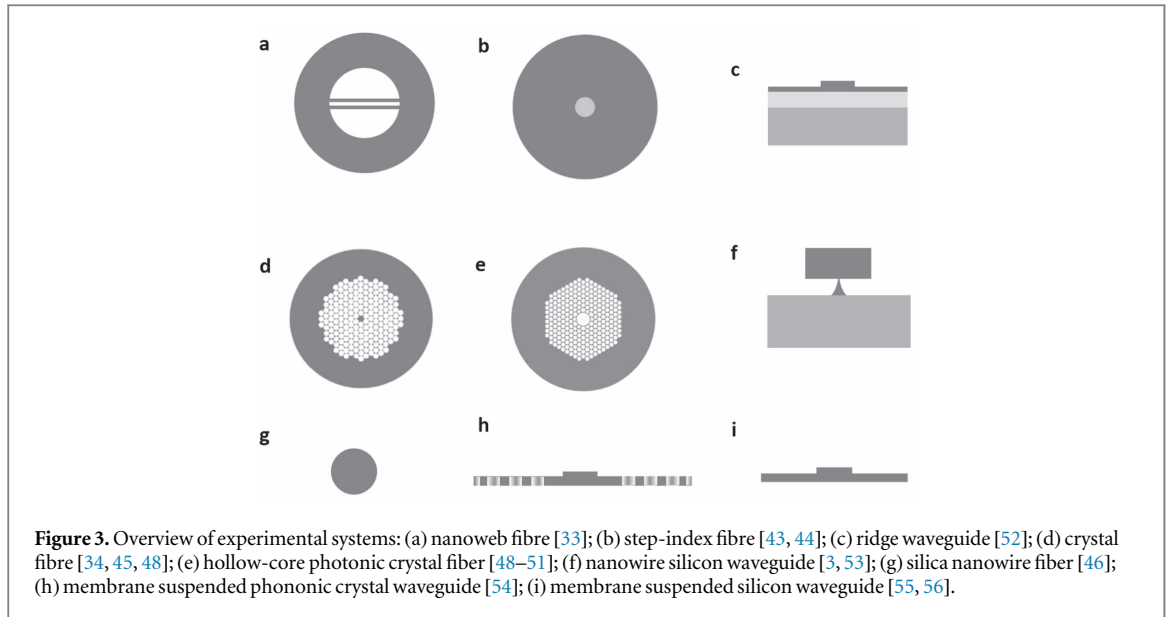
11. Experimental overview

We now discuss the experimental state-of-the-art in continuum optomechanics. Coupling between continuous optical and phonon fields has been realized in systems (figure 3) that include step-index and micro-structured optical fibers [33, 34, 43, 44–47], gas- and superfluid-filled photonic bandgap fibers [48–51], and chip-scale integrated optomechanical waveguides [3, 52, 53, 54–56]. These studies have overwhelmingly focused on Brillouin related nonlinear optical phenomena [3, 33, 34, 43, 44, 52, 45, 49, 50, 53, 46, 54–56, 47, 51], as well as noise processes [10, 48, 57]. However, it is interesting to examine these systems through the lens of continuum optomechanics. Figure 4(a) shows the estimated continuum-optomechanical couplings, extracted using the Brillouin gain G_B (see previous section). Couplings of 10^2 – 10^4 Hz $\text{m}^{1/2}$ have been realized using radiation pressure and/or photoelastic coupling. The phonon frequencies range from 10 MHz to 16 GHz, depending on the type of interaction (intra-band or inter-band) and the elastic wave mediating the coupling.

The strength of the nonlinear optical susceptibility increases linearly with phononic Q -factor. This is seen by comparing the effective phononic Q -factors (defined as the ratio of mechanical frequency and linewidth), plotted in figure 4(b), with the peak Brillouin gain of figure 4(c). The effective Q -factor is always smaller than the intrinsic Q -factor due to inhomogeneous broadening from spatial variations in waveguide dimension [59].

A variety of single-band (intra-modal) and multi-band (inter-modal) interactions have been demonstrated. The single-band processes include intra-modal forward-SBS processes (also termed stimulated Raman-like scattering, SMLS) and backward-SBS processes; each process is denoted with circular and square markers, respectively, in figure 4. Multi-band processes, generically termed inter-modal Brillouin processes, are denoted by triangles (see appendix D for their classification).

The phonon coherence length can vary dramatically. For instance, since intra-modal coupling is mediated by phonons with vanishing group velocities ($\sim 1 \text{ m s}^{-1}$) [55], coherence lengths are often less than 100 nm. Conversely, in the cases of backward- or inter-modal (inter-band) coupling, the phonon group velocities can



approach the material’s sound velocity (e.g., 10^4 m s^{-1}). This leads to 10–50 μm coherence lengths at room temperatures, but can be extended to millimeter length-scales at cryogenic temperatures [44].

Numerous proposed nano-optomechanical devices have the potential to yield increased coupling strengths [39, 60, 61]. Figure 5 indicates the prospects for exploring the strong coupling regime introduced above. In this table, we list the achievable coupling strengths for current and future continuum optomechanics experiments. We also take into account the phonon damping rate to estimate the threshold for the strong coupling regime in these structures. Both the ‘nanoweb’ photonic fibre structures and SIMS in silicon at cryogenic temperatures should enable observation of this regime.

System	coupling [Hz]	threshold [Hz]	frequency
“nanoweb” a	$10^6 - 10^7$	$2 \cdot 10^6$	5 MHz
silica fibre (cryo) b	$5 \cdot 10^7$	$2 \cdot 10^8$	9 GHz
SIMS Si c	$5 \cdot 10^8$	$9 \cdot 10^9$	6 GHz
SIMS Si (cryo) d	$5 \cdot 10^8$	$9 \cdot 10^6$	1 GHz

Figure 5. Possible experimental access to the strong coupling regime: the coupling $|\tilde{g}_{21}|$ needs to be much larger than the ‘threshold’ $\sqrt{v_2/v_b}\Gamma/4$. Estimated values for (a) [35], (b) [44], (c) stimulated intermodal scattering (SIMS) in silicon (room temp.) [58], (d) considers same system [58] at 1 K wherein Brillouin active phonon mode at 1 GHz is used and Q factors increase by a factor of 100 at low temperatures.

12. Conclusions

We have established a connection between the continuum limit of optomechanical arrays and Brillouin physics. Especially studies of (classical and quantum) nonlinear dynamics will profit from our approach, where we categorized the simplest coupling terms and derived the quantum Langevin equations, including the noise terms and the correct boundary conditions. Applications such as wavelength conversion, phonon-induced coherent photon interactions (as discussed recently in [62]) and extensions to two-dimensional situations [63, 64] can now be analyzed on the basis of this framework. As an example, we have discussed the strong coupling regime in continuum-optomechanical systems and prospects for reaching it in the context of state-of-the-art experimental systems.

Acknowledgments

We thank Philip Russell and Andrey Sukhorukov for initial discussions that helped inspire this project and for useful feedback on the manuscript. We acknowledge support by an ERC Starting Grant, as well as the European networks HOT and ITN OMT (FM). PTR acknowledges support from the Packard Fellowship for Science and Engineering.

Appendix A. Linearized interaction

We briefly review the (straightforward) route from the fully nonlinear interaction to the linearized version, i.e. a quadratic Hamiltonian. Assume a steady-state solution has been found, with $\beta(x) = \langle \hat{b}(x) \rangle$ and $\alpha(x) = \langle \hat{a}(x) \rangle$. As is known for standard cavity optomechanics, there might be more than one steady-state solution, and formally there could be an infinity of solutions for the continuum case. We have not explored this possibility further.

The deviations from this solution will now be denoted $\delta\hat{b} = \hat{b} - \beta$ and $\delta\hat{a} = \hat{a} - \alpha$. These are still fields. In contrast to the standard single-mode case, we will keep the possibility that $\beta(x)$ depends on position.

On the Hamiltonian level, we now obtain a new ‘linearized’ (i.e. quadratic) interaction term:

$$-\hbar \int dx [\tilde{g}(x) \delta\hat{a}^\dagger(x) + \tilde{g}^*(x) \delta\hat{a}(x)] [\delta\hat{b}(x) + \delta\hat{b}^\dagger(x)] \quad (36)$$

as well as a term

$$-\hbar \int dx \tilde{g}_\beta(x) \delta\hat{a}^\dagger(x) \delta\hat{a}(x), \quad (37)$$

which is a (possibly position-dependent) shift of the optical frequency. Its counterpart in the cavity optomechanics case is often dropped by an effective redefinition of the laser detuning.

In writing down equation (36), we have defined

$$\tilde{g}(x) \equiv \tilde{g}_0 \alpha(x) \quad (38)$$

$$\tilde{g}_\beta(x) \equiv \tilde{g}_0(\beta(x) + \beta^*(x)). \quad (39)$$

The photon-enhanced continuum coupling strength $\tilde{g}(x)$ is the direct analogue of the enhanced coupling $g = g_0\alpha$ in the standard linearized cavity-optomechanical case. In contrast to \tilde{g}_0 , \tilde{g} has the dimensions of a frequency. Likewise, \tilde{g}_β is the static mechanical displacement, expressed as a resulting optical frequency shift.

At this point, we have only started from the simplest kind of interaction, equation (2) of the main text, to obtain equation (36). Analogous (but lengthy) calculations can be provided starting from the other possible interaction terms of table 1 in the main text.

Appendix B. Optomechanical arrays: derivative terms in the continuum version of the interaction

In an optomechanical array, it is possible to have an interaction that creates phononic excitations during the photon tunneling process: $-\hbar g_0 (\hat{a}_{j+1}^\dagger \hat{a}_j + \text{h.c.}) \hat{u}_j$, where $\hat{u}_j \equiv \hat{b}_j + \hat{b}_j^\dagger$ describes the phonon displacement of a mode attached to the link between the sites j and $j + 1$. Here we describe how this can give rise to the canonical derivative terms when switching to a continuum description.

Switching from the discrete lattice model to the continuum model, we replace

$$\hat{a}_{j+1}^\dagger \hat{a}_j \hat{u}_j \mapsto \delta x^{3/2} \hat{a}^\dagger(x + \delta x/2) \hat{a}(x - \delta x/2) \hat{u}(x), \quad (40)$$

where we chose coordinates so as to indicate that the phonon mode \hat{u} is located halfway between the photon modes at $x \pm \delta x/2$. A Taylor expansion of

$$\hat{a}^\dagger(x + \delta x/2) \hat{a}(x - \delta x/2) + \text{h.c.} \quad (41)$$

yields

$$2\hat{a}^\dagger \hat{a} + \left(\frac{\delta x}{2}\right)^2 \{(\partial_x^2 \hat{a}^\dagger) \hat{a} + \hat{a}^\dagger (\partial_x^2 \hat{a}) - 2(\partial_x \hat{a}^\dagger)(\partial_x \hat{a})\}, \quad (42)$$

where all fields are taken at position x . Two things are worth noting here: first, all the first-order derivatives have disappeared (they would have violated inversion symmetry!). Second, we have obtained second-order derivatives of the photon field. If we want to turn this into our ‘canonical’ choice of coupling terms (table 1 of the main text), we have to integrate by parts, in which case derivatives may also act on $\hat{u}(x)$. This turns $\{(\partial_x^2 \hat{a}^\dagger) \hat{a} + \hat{a}^\dagger (\partial_x^2 \hat{a})\} \hat{u}$ into:

$$-2(\partial_x \hat{a}^\dagger)(\partial_x \hat{a}) \hat{u} - [(\partial_x \hat{a}^\dagger) \hat{a} + \hat{a}^\dagger (\partial_x \hat{a})](\partial_x \hat{u}). \quad (43)$$

Combining this with the other terms resulting from equation (42), one arrives at the interaction expressed completely in the canonical way.

Appendix C. Nonlinear susceptibility

We briefly discuss how, starting from the linearized equation (25) of the main text, we can obtain the effective third-order nonlinear photon susceptibility induced by the interaction with the phonons. We slightly generalize this equation, by adding a possible detuning between the mechanical frequency Ω and the transition frequency Ω_o between the two optical branches:

$$\partial_x \langle \delta \hat{b} \rangle = i[(\Omega - \Omega_o)/v_b] \langle \delta \hat{b} \rangle + i(\tilde{g}_{21}/v_b) \langle \delta \hat{a}_2^\dagger \rangle - (\gamma_b/2) \langle \delta \hat{b} \rangle. \quad (44)$$

Solving for the steady-state $\partial_x \langle \delta \hat{b} \rangle$ and inserting into the photon equation of motion, equation (25) of the main text, we obtain:

$$\partial_x \langle \delta \hat{a}_2 \rangle = -\frac{i}{v_2} \frac{|\tilde{g}_0(2,1)|^2 |\alpha_1|^2 \langle \delta \hat{a}_2 \rangle}{\Omega - \Omega_o - i\frac{\Gamma}{2}} - \frac{\gamma_2}{2} \langle \delta \hat{a}_2 \rangle. \quad (45)$$

We can express this as

$$\partial_x \langle \delta \hat{a}_2 \rangle = i\gamma_{\text{nonlin}}^{(3)} |\alpha_1|^2 \langle \delta \hat{a}_2 \rangle - \frac{\gamma_2}{2} \langle \delta \hat{a}_2 \rangle, \quad (46)$$

with the effective nonlinear susceptibility

$$\gamma_{\text{nonlin}}^{(3)}(\Omega) = -\frac{1}{v_2} \frac{|\tilde{g}_0(2,1)|^2}{\Omega - \Omega_o - i\frac{\Gamma}{2}}. \quad (47)$$

Using $P_1 = \hbar\omega_1 v_1 |\alpha_1|^2$ and $P_2 \cong \hbar\omega_2 v_2 |\langle \delta \hat{a}_2 \rangle|^2$ to cast equation (47) in the form of equation (28) of the main text, one finds that the frequency dependent gain is related to the nonlinear susceptibility as $G_B(\Omega) = -2 \cdot \text{Im}\{\gamma_{\text{nonlin}}^{(3)}(\Omega)\} (\hbar\omega_1 v_1)^{-1}$.

Appendix D. Types of Brillouin interactions

Here, we elucidate some naming conventions used in the Brillouin literature, and we explain how these names relate to the classifications that we use in this paper. These include (i) forward intra-band scattering processes, where incident and scattered light-fields co-propagate in the same optical mode, (ii) backward intra-band scattering processes, where the incident and scattered light-fields counter-propagate, as well as (iii) inter-band

scattering processes, which generically describe processes that involve coupling between guided optical modes with distinct dispersion curves. Note that within figure 4 of the main text processes (i), (ii), and (iii) are identified by circular, square, and triangular markers, respectively.

Backward intra-band scattering processes, which is the most widely studied of Brillouin interactions, is commonly termed backward stimulated Brillouin scattering [11, 12]; [43, 44, 52, 45, 46] are examples of this process. However, for historical reasons, the terminology for forward intra-band and forward inter-band scattering processes is somewhat more diverse. Thermally driven (or spontaneous) forward intra-band scattering was first observed in optical fibers, and identified as a noise process, under the name guided acoustic wave Brillouin scattering (GAWBS) [10]; [48, 57] are examples of this spontaneous process. Stimulated forward intra-band scattering processes have been described using the term (intra-modal) forward stimulated Brillouin scattering [3, 49, 50, 53, 54–56, 51], as well as using the more descriptive term SRLS [33, 47].

Inter-band processes have also been observed through both spontaneous and stimulated interactions under different names. Stimulated inter-band coupling between co-propagating guided optical modes with different polarization states has been termed stimulated inter-polarization scattering [47]. In the context of noise processes, the spontaneous version process has also been described using the term de-polarized GAWBS or depolarization scattering [48, 57]. Stimulated scattering between co-propagating guided optical modes with distinct spatial distribution has also been described using the term SIMS [35] and stimulated inter-modal Brillouin scattering [37].

ORCID iDs

Florian Marquardt  <https://orcid.org/0000-0003-4566-1753>

References

- [1] Aspelmeyer M, Kippenberg T J and Marquardt F 2014 Cavity optomechanics *Rev. Mod. Phys.* **86** 1391–452
- [2] Rakich P T, Reinke C, Camacho R, Davids P and Wang Z 2012 Giant enhancement of stimulated Brillouin scattering in the subwavelength limit *Phys. Rev. X* **2** 011008
- [3] Van Laer R, Kuyken B, Van Thourhout D and Baets R 2015 Interaction between light and highly confined hypersound in a silicon photonic nanowire *Nat. Photon.* **9** 199–203
- [4] Butsch A, Koehler J R, Noskov R E and Russell P S 2014 CW-pumped single-pass frequency comb generation by resonant optomechanical nonlinearity in dual-nanowire fiber *Optica* **1** 158
- [5] Li M *et al* 2008 Harnessing optical forces in integrated photonic circuits *Nature* **456** 480–4
- [6] Bahl G, Tomes M, Marquardt F and Carmon T 2012 Observation of spontaneous Brillouin cooling *Nat. Phys.* **8** 203–7
- [7] Bahl G *et al* 2013 Brillouin cavity optomechanics with microfluidic devices *Nat. Commun.* **4** 1994
- [8] Kim J, Kuzyk M C, Han K, Wang H and Bahl G 2015 Non-reciprocal Brillouin scattering induced transparency *Nat. Phys.* **11** 275–80
- [9] Shen Y R and Bloembergen N 1965 Theory of stimulated Brillouin and Raman scattering *Phys. Rev.* **137** A1787–805
- [10] Shelby R M, Levenson M D and Bayer P W 1985 Guided acoustic-wave Brillouin scattering *Phys. Rev. B* **31** 5244–52
- [11] Boyd R W 2013 *Nonlinear Optics* (New York: Academic)
- [12] Agrawal G 2012 *Nonlinear Fiber Optics* (New York: Academic)
- [13] Van Laer R, Baets R and Van Thourhout D 2016 Unifying Brillouin scattering and cavity optomechanics *Phys. Rev. A* **93** 053828
- [14] Laude V and Beugnot J-C 2015 Lagrangian description of Brillouin scattering and electrostriction in nanoscale optical waveguides *New J. Phys.* **17** 125003
- [15] Sipe J E and Steel M J 2016 A Hamiltonian treatment of stimulated Brillouin scattering in nanoscale integrated waveguides *New J. Phys.* **18** 045004
- [16] Zoubi H and Hammerer K 2016 Optomechanical multi-mode Hamiltonian for nanophotonic waveguides *Phys. Rev. A* **94** 053827
- [17] Kharel P, Behunin R O, Renninger W H and Rakich P T 2016 Noise and dynamics in forward Brillouin interactions *Phys. Rev. A* **93** 063806
- [18] Safavi-Naeini A H *et al* 2014 Two-dimensional phononic–photonic band gap optomechanical crystal cavity *Phys. Rev. Lett.* **112** 153603
- [19] Zhang M, Shah S, Cardenas J and Lipson M 2015 Synchronization and phase noise reduction in micromechanical oscillator arrays coupled through light *Phys. Rev. Lett.* **115** 163902
- [20] Chang D, Safavi-Naeini A H, Hafezi M and Painter O 2011 Slowing and stopping light using an optomechanical crystal array *New J. Phys.* **13** 023003
- [21] Chen W and Clerk A A 2014 Photon propagation in a one-dimensional optomechanical lattice *Phys. Rev. A* **89** 033854
- [22] Schmidt M, Peano V and Marquardt F 2015 Optomechanical Dirac physics *New J. Phys.* **17** 023025
- [23] Heinrich G, Ludwig M, Qian J, Kubala B and Marquardt F 2011 Collective dynamics in optomechanical arrays *Phys. Rev. Lett.* **107** 043603
- [24] Xuereb A, Genes C and Dantan A 2012 Strong coupling and long-range collective interactions in optomechanical arrays *Phys. Rev. Lett.* **109** 223601
- [25] Schmidt M, Ludwig M and Marquardt F 2012 Optomechanical circuits for nanomechanical continuous variable quantum state processing *New J. Phys.* **14** 125005
- [26] Xuereb A, Genes C, Pupillo G, Paternostro M and Dantan A 2014 Reconfigurable long-range phonon dynamics in optomechanical arrays *Phys. Rev. Lett.* **112** 133604
- [27] Ludwig M and Marquardt F 2013 Quantum many-body dynamics in optomechanical arrays *Phys. Rev. Lett.* **111** 073603
- [28] Schmidt M, Kessler S, Peano V, Painter O and Marquardt F 2015 Optomechanical creation of magnetic fields for photons on a lattice *Optica* **2** 635

- [29] Peano V, Brendel C, Schmidt M and Marquardt F 2015 Topological phases of sound and light *Phys. Rev. X* **5** 031011
- [30] Walter S and Marquardt F 2015 Dynamical gauge fields in optomechanics *New J. Phys.* **18** 113029
- [31] Sarabalis C J, Hill J T and Safavi-Naeini A H 2016 Guided acoustic and optical waves in silicon-on-insulator for Brillouin scattering and optomechanics *APL Photonics* **1** 071301
- [32] Wolff C, Stiller B, Eggleton B J, Steel M J and Poulton C G 2016 Cascaded forward Brillouin scattering to all Stokes orders *New J. Phys.* **19** 023021
- [33] Butsch A *et al* 2012 Optomechanical nonlinearity in dual-nanoweb structure suspended inside capillary fiber *Phys. Rev. Lett.* **109** 183904
- [34] Kang M S, Nazarkin A, Brenn A and Russell P S J 2009 Tightly trapped acoustic phonons in photonic crystal fibres as highly nonlinear artificial Raman oscillators *Nat. Phys.* **5** 276–80
- [35] Koehler J R *et al* 2016 Resolving the mystery of milliwatt-threshold opto-mechanical self-oscillation in dual-nanoweb fiber *APL Photonics* **1** 056101
- [36] Chiao R Y, Townes C H and Stoicheff B P 1964 Stimulated Brillouin scattering and coherent generation of intense hypersonic waves *Phys. Rev. Lett.* **12** 592–5
- [37] Qiu W *et al* 2013 Stimulated Brillouin scattering in nanoscale silicon step-index waveguides: a general framework of selection rules and calculating SBS gain *Opt. Express* **21** 31402–19
- [38] Wolff C, Steel M J, Eggleton B J and Poulton C G 2015 Stimulated Brillouin scattering in integrated photonic waveguides: forces, scattering mechanisms, and coupled-mode analysis *Phys. Rev. A* **92** 013836
- [39] Qiu W, Rakich P T, Shin H, Dong H, Soljačić M and Wang Z 2013 Stimulated Brillouin scattering in nanoscale silicon step-index waveguides: a general framework of selection rules and calculating SBS gain *Opt. Express* **21** 31402–19
- [40] Renninger W H, Kharel P, Behunin R O and Rakich P T 2018 Bulk crystalline optomechanics *Nat. Phys.* (<https://doi.org/10.1038/s41567-018-0090-3>)
- [41] Zhu Z, Gauthier D J and Boyd R W 2007 Stored light in an optical fiber via stimulated Brillouin scattering *Science* **318** 1748–50
- [42] Chen Y-C, Kim S and Bahl G 2016 Brillouin cooling in a linear waveguide *New J. Phys.* **18** 115004
- [43] Abedin K S 2005 Observation of strong stimulated Brillouin scattering in single-mode As_2Se_3 chalcogenide fiber *Opt. Express* **13** 10266–71
- [44] Behunin R O 2015 Long-lived guided phonons in fiber by manipulating two-level systems arXiv:1501.04248
- [45] Beugnot J-C, Sylvestre T, Maillotte H, Mélin G and Laude V 2007 Guided acoustic wave Brillouin scattering in photonic crystal fibers *Opt. Lett.* **32** 17
- [46] Beugnot J-C *et al* 2014 Brillouin light scattering from surface acoustic waves in a subwavelength-diameter optical fibre *Nat. Commun.* **5** 5242
- [47] Kang M S, Brenn A St and Russell P St J 2010 All-optical control of gigahertz acoustic resonances by forward stimulated inter-polarization scattering in a photonic crystal fiber *Phys. Rev. Lett.* **105** 153901
- [48] Zhong W E N *et al* 2015 Depolarized guided acoustic wave Brillouin scattering in hollow-core photonic crystal fibers *Opt. Express* **23** 27707
- [49] Renninger W H, Behunin R and Rakich P 2016 Nonlinear optics in superfluid helium-filled hollow-core fiber *CLEO: QELS Fundamental Science* (Optical Society of America)
- [50] Renninger W H *et al* 2016 Forward Brillouin scattering in hollow-core photonic bandgap fibers *New J. Phys.* **18** 025008
- [51] Renninger W H, Behunin R O and Rakich P T 2016 Guided-wave Brillouin scattering in air *Optica* **3** 1316–9
- [52] Pant R 2010 On-chip stimulated Brillouin scattering *Opt. Express* **18** 19286–91
- [53] Laer R V, Bazin A, Kuyken B, Baets R and Thourhout D V 2015 Net on-chip Brillouin gain based on suspended silicon nanowires *New J. Phys.* **17** 115005
- [54] Shin H *et al* 2015 Control of coherent information via on-chip photonic-phononic emitter-receivers *Nat. Commun.* **6** 6427
- [55] Shin H *et al* 2013 Tailorable stimulated Brillouin scattering in nanoscale silicon waveguides *Nat. Commun.* **4** 1944
- [56] Kittlaus E A, Shin H and Rakich P T 2016 Large Brillouin amplification in silicon *Nat. Photon.* **10** 463–7
- [57] Elser D *et al* 2006 Reduction of guided acoustic wave Brillouin scattering in photonic crystal fibers *Phys. Rev. Lett.* **97** 133901
- [58] Kittlaus E A, Otterstrom N T and Rakich P T 2017 On-chip inter-modal Brillouin scattering *Nat. Commun.* **8** 15819
- [59] Wolff C, Laer R V, Steel M J, Eggleton B J and Poulton C G 2016 Brillouin resonance broadening due to structural variations in nanoscale waveguides *New J. Phys.* **18** 025006
- [60] Van Laer R, Kuyken B, Van Thourhout D and Baets R 2014 Analysis of enhanced stimulated Brillouin scattering in silicon slot waveguides *Opt. Lett.* **39** 1242–5
- [61] Sarabalis C J, Hill J T and Safavi-Naeini A H 2016 Guided acoustic and optical waves in silicon-on-insulator for Brillouin scattering and optomechanics *APL Photonics* **1** 071301
- [62] Zoubi H and Hammerer K 2016 Nonlinear quantum optics in optomechanical nanoscale waveguides *Phys. Rev. Lett.* **119** 123602
- [63] Ruiz-Rivas J, Navarrete-Benlloch C, Patera G, Roldán E and de Valcárcel G J 2016 Dissipative structures in optomechanical cavities *Phys. Rev. A* **93** 033850
- [64] Butsch A, Conti C, Biancalana F and Russell P S 2012 Optomechanical self-channeling of light in a suspended planar dual-nanoweb waveguide *Phys. Rev. Lett.* **108** 093903